Proceedings of the International Conference "Quantum Optics V", Kościelisko, Poland, 2001

On the Extinction Paradox

W. Żakowicz

Institute of Physics, Polish Academy of Sciences
al. Lotników 32/46, Warsaw 02-668, Poland

The extinction paradox, the difference of classical and quantum scattering cross-sections for the scattering of particles by a rigid sphere ($\sigma^{\mathrm{Q}} = 2\pi a^2 = 2\sigma^{\mathrm{C}}$ for $ka \gg 1$), is analyzed in a simpler 2D model of a rigid cylindrical potential. Rigorous solutions of the Schrödinger equation for particle beams, including also finite width beams, are derived and employed in the description of the scattering process. The scattering particle fluxes, with a thorough treatment of the forward directions, are being studied. It is pointed out that for wide beams ($w \gg a$) the scattered flux can reach the value determined by the quantum theory, provided that it is measured at distances $R \gg wa\lambda$. Moderately narrow beams ($1 \ll w \ll a$) behave as classical trajectories, and their scattering can be described in classical terms. Thus, the classical limit of quantum scattering requires not only that the de Broglie wavelength λ_{B} is much smaller than the size of the scatterer ($a \gg \lambda_{\mathrm{B}}$), but also that the transverse width of beams of de Broglie's waves is small, $w \ll a$.

PACS numbers: 32.80.Cy, 42.25.Fx, 61.10.Dp

1. Introduction

Almost all textbooks on quantum mechanics, e.g. [1–3], as well as the scattering theory, e.g. [4, 5], discuss the scattering of a particle by an impenetrable sphere and show that for large particle momenta $ka \gg 1$ the cross-section is twice its geometrical cross-section area πa^2. For the first time this result has been obtained by Massey and Mohr [6]. The condition of large particle momenta means that the de Broglie wavelength λ_{B} is much smaller than the radius of the scatterer a. This is considered as the necessary condition for the classical limit of quantum mechanics, so, the above result seems paradoxical. Therefore, it is referred to as the "extinction paradox".

A similar effect exists also for the scattering of electromagnetic waves by a conducting sphere in the limit of short wavelength, $\lambda \ll a$ [7].

The effect has been interpreted as caused by the interference of the waves diffracted and passing near the sharp boundary of a scattering potential. It is believed that for a diffused boundary the cross-section in the limit $ka \gg 1$ should match the classical value; however, this assumption still needs a quantitative verification. In this discussion, which is again devoted to a rigid boundary scatterer model, a more careful treatment is given to the description of incident beams of a finite width and to the determination of particle flux in the directions overlapping with the incident beam.

2. Classical and quantum two-dimensional scattering by a perfectly reflecting cylinder

To contribute to this discussion let us consider an exactly solvable, in the classical and the quantum theories, scattering model. The model consists of a hard, perfectly reflecting cylinder with incident particles perpendicular to and uniform along the cylinder. In this configuration all dynamical equations, either the classical equations of motion, or the Schrödinger equation in the quantum case, reduce to the two-dimensional problems that can be solved exactly.

The definition and description of scattering in both theories are different. In the classical picture the trajectories of scattered or deflected particles can be easily distinguished from those non-scattered. The scattering angle ϕ of each incident particle depends only on the impact parameter. Within the quantum mechanical approach wave functions give only statistical information about scattering of an ensemble of the particles. One definitely cannot determine whether a particular particle is deflected and scattered. There is no relation between the scattering angle and the impact parameter, as this parameter is not determined. On the other hand, the quantum description of scattering are very often given in terms of phase shifts, which are not defined and present in the classical theories. Therefore, it is rather difficult to compare the classical and the quantum scattering theories as both theories have different notions of the scattering and describe it using different terms and variables.

Attempting to make a comparison of both theories we may first ask two questions:

1) is the limit of de Broglie's wavelength $\lambda_{\mathrm{B}} \ll a$ the sufficient condition for the classical scattering?

2) what conditions are required for the observation of the quantum scattering?

To answer these questions and to relate the quantum and the classical theories let us consider an exactly soluble in both theories two-dimensional model of the scattering of a particles by a 2D cylindrical potential infinite step (rigid cylinder) of radius a.

As it is well known, the scattering of a plane wave by a rigid sphere can be also solved exactly [1–5]. The hard cylinder model has been chosen because

it is simpler and the description of confined and displaced beams is easier than for spheres. Assuming that the incident beams are uniform along the cylinder the model can be formulated as a two-dimensional problem.

2.1. Classical scattering

For a hard cylinder scatterer in the classical mechanics, sketched in Fig. 1, only the reflection law, i.e. the inversion of the normal component of velocity at the moment of collision is necessary to determine a dependence of the scattering angle ϕ on the impact parameter ρ:

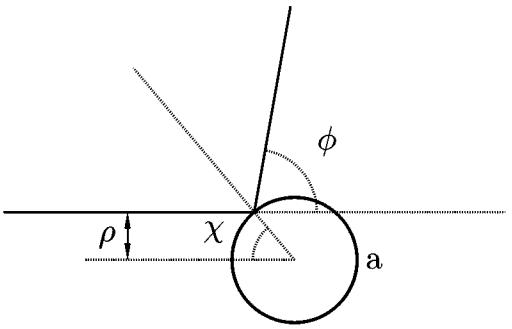

Fig. 1. Particle trajectory in classical scattering from a rigid cylinder.

$$\phi = \pi - 2\arcsin\rho/a,$$

leading to the differential cross-section

$$\frac{\mathrm{d}\sigma^{\mathrm{C}}}{\mathrm{d}\phi} = \frac{a}{2}\sin\frac{\phi}{2}. \tag{1}$$

Thus, only the particles coming with $|\rho| < a$ are scattered and the total cross-section is

$$\sigma_0^{\mathrm{C}} = \int_{-\pi}^{\pi} \frac{\mathrm{d}\sigma^{\mathrm{C}}}{\mathrm{d}\phi}\mathrm{d}\phi = 2a. \tag{2}$$

2.2. Quantum scattering

The quantum description of the scattering can be extracted from the stationary wave functions satisfying the time independent Schrödinger equation. For incident particles propagating toward a scatterer placed at the origin of the coordinate system along the direction $\hat{\boldsymbol{k}}(\alpha) = \{\cos\alpha, \sin\alpha, 0\}$ and described by the corresponding plane wave, the total wave function, satisfying the necessary boundary condition $\Psi(a) = 0$, is

$$\Psi_{\mathrm{T}}(\boldsymbol{r}) = \Psi_{\mathrm{I}} + \Psi_{\mathrm{S}} = \mathrm{e}^{\mathrm{i}\boldsymbol{k}(\alpha)\cdot\boldsymbol{r}} - \sum_{n=-\infty}^{\infty} \mathrm{i}^n \mathrm{e}^{-\mathrm{i}n\alpha}\mathrm{e}^{\mathrm{i}n\phi}\frac{J_n(ka)}{H_n^{(1)}(ka)}H_n^{(1)}(kr), \tag{3}$$

where J_n and $H_n^{(1)}$ are the Bessel and Hankel functions of order n; they can be computed using Bessel's functions libraries. Although the sum includes the infinite number of terms, when a is finite, only the finite number of terms are necessary to reach the required accuracy. Figures 2a and b illustrate the magnitude of the partial wave amplitudes and the reached accuracy of boundary condition for the scatterer of radius $a = 25$ (all sizes and distances are given in the de Broglie wavelength unit). Taking into account 2×220 partial waves the wave function at $r = a$ is of the order of $\approx 10^{-13}$ and the corresponding wave function can be considered to be exact.

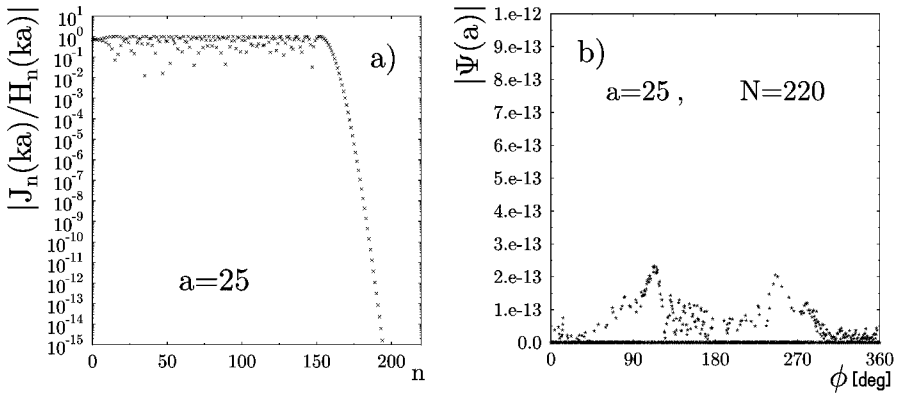

Fig. 2. (a) Magnitude of partial wave expansion coefficients, (b) accuracy in the fulfillment of the boundary condition, $a = 25\lambda$.

Knowing the incident, scattered, and total wave functions we can calculate the corresponding particle currents

$$\boldsymbol{J}_Q(\boldsymbol{r}) = \frac{\hbar}{m} \Re e \Psi_Q(\boldsymbol{r}) \mathrm{i} \nabla \Psi_Q^*(\boldsymbol{r}), \tag{4}$$

and the radial fluxes

$$F_Q^r(r, \phi) = \int_0^{\phi} J_Q^r(r, \phi') \mathrm{d}\phi', \tag{5}$$

where Q stands for {I, S, T} depending whether one takes either the incident or the scattered part or the total wave function.

An example of the radial components of the currents and fluxes is shown in Figs. 3a and b. While at this distance J_{T}^r vanishes in the forward directions $\phi < 10°$ (which corresponds to a shadow behind the scatterer) it oscillates around J_{I}^r with increasing ϕ-frequency and decreasing amplitude. The scattered current J_{S}^r is strongly peaked in the forward directions while beyond this forward sector it remains rather small.

The currents J_{I}^r and J_{T}^r integrated over all angles i.e. the fluxes $F_{\mathrm{I}}^r(\pi)$ and $F_{\mathrm{T}}^r(\pi)$ vanish in agreement with the unitary properties of the wave function. Only

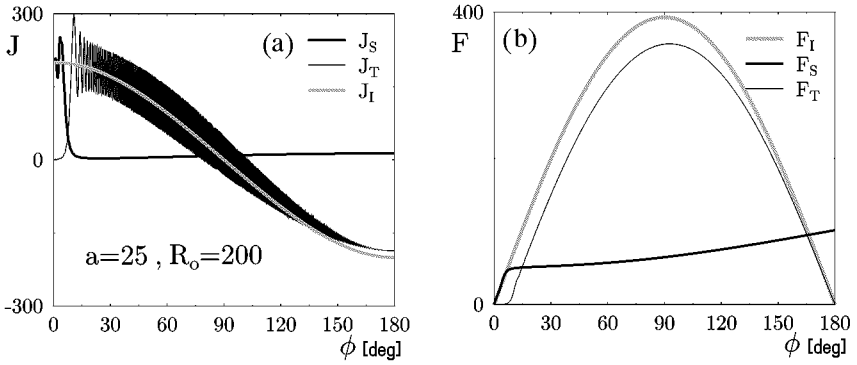

Fig. 3. (a) Incident, scattered and total radial currents for the plane wave scattering as functions of the scattering angle θ. (b) The same for fluxes. F and J are in arbitrary units.

the scattered current J_S^r integrated over all angles, i.e. $F_S^r(\pi)$, is non-vanishing. It is this object that is used to estimate and evaluate the interaction between the incident particles and the target particle causing scattering.

An important property of the scattering process is characterized by a differential cross-section

$$\left(\frac{\mathrm{d}\sigma}{\mathrm{d}\phi}\right) \propto r J_S^r, \tag{6}$$

and a total cross-section

$$\sigma_0 = \int_{-\pi}^{\pi} \left(\frac{\mathrm{d}\sigma}{\mathrm{d}\phi}\right) \mathrm{d}\phi. \tag{7}$$

When the above definitions are applied to the scattered part of the wave function (3), in the limit $ka \gg 1$ we obtain

$$\sigma_0^{\mathrm{Q}} \to 4a, \tag{8}$$

so we have $\sigma_0^{\mathrm{Q}} = 2\sigma_0^{\mathrm{C}}$.

The above procedure summarizes the basic features of the quantum mechanical derivation of the parameter known as the scattering cross-section. This procedure can be found in all textbooks on the quantum mechanics. It is clear, simple and leads to the object having many interesting and useful properties, e.g.: no interferences between different partial waves contributions in the total cross-section, a simple form of the optical theorem that relates σ_0^{Q} with properties of Ψ_S in the forward direction. However, the usage of J_S raises some questions.

Can $\boldsymbol{J}_S(\boldsymbol{r})$ always represent a flux of particles? The function $\Psi_S(\boldsymbol{r})$ is only a part of the quantum wave function. Can the Born interpretation of the wave function with $\rho = \Psi^*\Psi$ treated as the density of particles be extended to the part of the wave function, $\rho_S = \Psi_S^*\Psi_S$?

Within the orthodox formulation of the quantum mechanics the process of scattering should be described by the measurable quantities and such are those expressed by Ψ_{I} and Ψ_{T} , i.e. $\boldsymbol{J}_{\mathrm{I}}$ and $\boldsymbol{J}_{\mathrm{T}}$. Both quantities represent the true particle wave functions giving the true particle densities and currents. While Ψ_{I} and $\boldsymbol{J}_{\mathrm{I}}$ refer to particle beams without any scatterer (or scatterer removed) then with the scatterer presence the wave function is different and is described by Ψ_{T} determining $\boldsymbol{J}_{\mathrm{T}}$. In the following it is shown how the above program can be realized. Before this will be done let us point out two difficulties in operating with $\boldsymbol{J}_{\mathrm{T}}$.

Firstly, as can be seen in Fig. 3 the current $J_{\mathrm{T}}^{r}(r,\phi)$ is a rapidly varying function of ϕ, and such rapid variations may be difficult for measurements.

Secondly, we can recall an independent description and visualization of the scattering, proposed by Hirschfelder et al. [8], given in terms of flow lines, which are the lines tangent to the current field $\boldsymbol{J}_{\mathrm{T}}(\boldsymbol{r})$. In the case of electrodynamics the flow lines are tangent to the Poynting field which has been recently discussed in [9]. The flow lines can be obtained by solving a set of the differential equations

$$\frac{\mathrm{d}\boldsymbol{r}}{\mathrm{d}\tau} = \boldsymbol{J}_{\mathrm{T}}(\boldsymbol{r}(\tau)). \tag{9}$$

Solving this set of equations with the help of any Runge–Kutta type methods, with the initial data $\boldsymbol{r}(0) = \boldsymbol{r}_0$, the integrated flow lines can be found. Such flow lines, corresponding to the scattering by the hard cylinder of radius $a = 10$, are shown in Fig. 4. The incident particles are coming from the left side where far away the

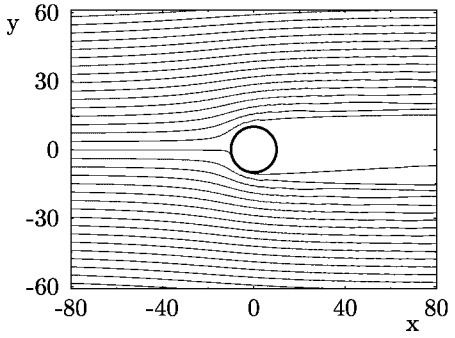

Fig. 4. Flow lines for the plane wave scattering, $a = 10\lambda$.

flow is uniform and the flow lines are parallel. Sampling this flow field at equal spacing the fluxes embraced between two consecutive lines are equal. The particles which are overflowing the scatterer leave a wake, void track visible as a shadow behind the scatterer. The flow lines representing the integrated solutions of the differential equations can neither intersect nor split. It is puzzling that these flow lines do not show any large angle scatterings. That is in a complete disagreement with our expectations and observations.

To get a consistent description of scattering the incident uniform flux of particles represented by the plane wave must be replaced by the particle beams

having a finite transverse width and represented by the appropriate wave function. In fact, all scattering experiments are performed with finite width beams. Outside the incident beams we have

$$\Psi_{\mathrm{S}} = \Psi_{\mathrm{T}}, \quad \text{and} \quad \boldsymbol{J}_{\mathrm{S}} = \boldsymbol{J}_{\mathrm{T}},$$

so the differential cross-section formula, Eq. (6), raises no questions if it is used for the particles outside the incident beam. However, defining the total cross-section σ_0, Eq. (7), through the integration over all the scattering angles the integral includes also the disputed sector. One may hope that this disputed contribution is negligible if the scattered particles are observed at sufficiently large distances from the scatterer. In the following we investigate this assumption quantitatively.

3. Gaussian beams scattering

The wave function given by Eq. (3) corresponds to the incident plane wave propagating at an angle α with respect to the x-axis. Superposing the wave functions with different angles α wave functions for finite width beams can be found.

Thus, the incident plane wave must be replaced by

$$\mathrm{e}^{\mathrm{i}\boldsymbol{k}(\alpha)\cdot\boldsymbol{r}} \Longrightarrow \int \mathrm{d}\alpha \mathrm{e}^{\mathrm{i}\boldsymbol{k}(\alpha)\cdot(\boldsymbol{r}-\boldsymbol{r}_0)} P(\alpha), \tag{10}$$

while in the scattered part of the wave function the factor $\mathrm{e}^{-\mathrm{i}n\alpha}$ must be replaced by

$$\mathrm{e}^{-\mathrm{i}n\alpha} \Longrightarrow \int \mathrm{d}\alpha \mathrm{e}^{-\mathrm{i}n\alpha} \mathrm{e}^{-\mathrm{i}\boldsymbol{k}(\alpha)\cdot\boldsymbol{r}_0} P(\alpha), \tag{11}$$

where for a Gaussian beam model the angular distribution function

$$P(\alpha) = \frac{w}{\sqrt{\pi}} \mathrm{e}^{-w^2\alpha^2},$$

and w is a parameter determining the angular spread of the incident beam, as well as its spatial width, while $\boldsymbol{r}_0$ determines the position of the Gaussian beam waist.

This form of the incident beam wave function is not very convenient in any further computations because it requires the integration at each point $\boldsymbol{r}$.

It is worth pointing out that this inconvenience concerns the incident beam only. The scattered part of the wave function requires the modified, according to Eq. (11), partial wave expansion coefficients. However, all these coefficients, and therefore integrations, have to be computed only once.

To avoid problems introduced by the above integrations two approximations can be proposed. In the first one, the integrals are replaced by the sums over the discrete plane waves,

$$\int \mathrm{d}\alpha P(\alpha) \ldots \longrightarrow \sum_i P(\alpha_i) \ldots$$

The second approximation is valid for beams with a small angular spread, and therefore for rather wider beams, $w \gg 1$. For these beams $\boldsymbol{k}(\alpha)$ can be approximated by the lowest order terms $\boldsymbol{k}(\alpha) \approx k\{1 - \alpha^2/2, \alpha, 0\}$ and all the necessary

integrations with $P(\alpha)$ can be done analytically. Thus we get, for the freely propagating incident wave,

$$\Psi_{\mathrm{I}}(x,y) \approx \frac{2w}{\sqrt{4w^2+2\mathrm{i}k(x-x_0)}}\mathrm{e}^{\mathrm{i}k(x-x_0)}\exp\left[-\frac{k^2(y-y_0)^2}{4w^2+2\mathrm{i}k(x-x_0)}\right], \qquad (12)$$

and for the modification factors for the partial wave expansion coefficients,

$$\langle \mathrm{e}^{\mathrm{i}n\alpha}\mathrm{e}^{\mathrm{i}\boldsymbol{k}(\alpha)\cdot\boldsymbol{r}_0}\rangle \approx \frac{2w}{\sqrt{4w^2-2\mathrm{i}kx_0}}\mathrm{e}^{-\mathrm{i}kx_0}\exp\left[-\frac{(n+ky_0)^2}{4w^2-2\mathrm{i}kx_0}\right]. \qquad (13)$$

These approximations introduce some errors in the solutions of the Schrödinger equation. The first approximation, though still keeping the boundary conditions fulfilled, introduces spurious "ghost" beams that propagate in the same direction as the beam, and are repeated periodically along the orthogonal direction. The freely propagating beams in the second approximation are not exact solutions of the Schrödinger equation, so the full wave functions cannot be claimed to be exact. Nevertheless, their accuracy can be very good, particularly for the wide beams.

In Fig. 5 the flow lines for the scattered incident beam of finite width are shown. In this case there is also the shadow region behind the scatterer; however, there are the flow lines representing large angle scatterings. These large angle scattering lines are connected with the peripheral lines in the wings of the incident beam. This property is completely different from that for the classical trajectories. Classically, the incident particles moving with smaller impact parameter are more deflected. The flow lines introduced in this discussion are illustrating global properties of the wave solutions of the scattering problem.

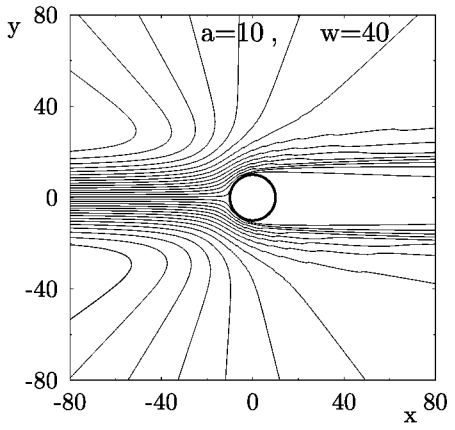

Fig. 5. Flow lines for the finite width beam scattering.

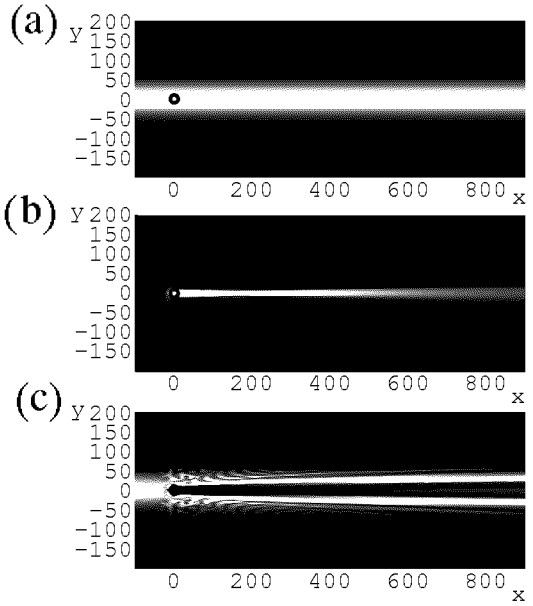

Fig. 6. Density plots for modulus of the currents: (a) incident ($|\boldsymbol{J}_{\mathrm{I}}|$), (b) scattered ($|\boldsymbol{J}_{\mathrm{S}}|$), (c) total ($|\boldsymbol{J}_{\mathrm{T}}|$) as functions of the $x-y$ coordinates ($a = 10,\ w = 60$).

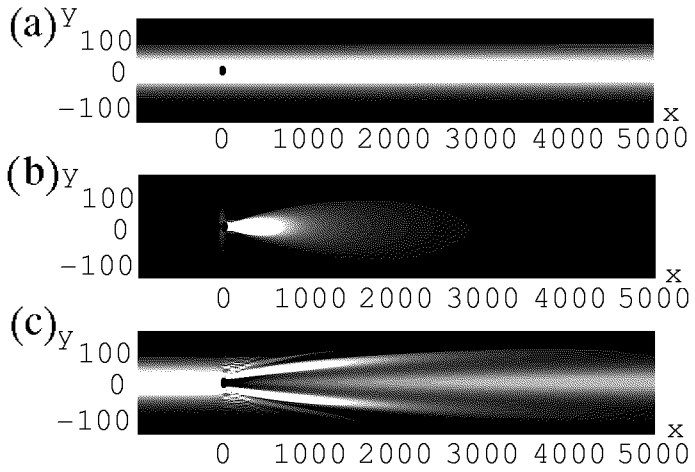

Fig. 7. Similar as in Fig. 6, with faster spreading of the scattered wave function, over a longer distance ($a = 5,\ w = 100$).

Figures 6 and 7 show the density plots representing the magnitudes of the discussed currents: incident $|\boldsymbol{J}_{\mathrm{I}}(\boldsymbol{r})|$ (top figures), scattered according to the scattered part of the wave function $|\boldsymbol{J}_{\mathrm{S}}(\boldsymbol{r})|$ (middle figures) and scattered according to the total wave function $|\boldsymbol{J}_{\mathrm{T}}(\boldsymbol{r})|$ (bottom figures).

As it is seen, the scattering current computed according to the scattering part of the wave function is dominated by a very strong peak in the forward direction, while the scattering current beyond this forward sector is hardly visible. However, this huge flux in the forward direction, when it overlaps with the incident beam, does not represent any flux of particles, and is not a measurable quantity. The scattered part of the wave function is only a subsidiary function that can be computed and used to find the complete wave function. As the bottom figures show, these big scattered parts of the wave functions contribute to the complete shadows just behind the scatterers. These shadow regions, in which no particles can be detected, are surrounded by a transition region where the particle currents exhibit strong transverse modulations. These oscillations appear on a screen placed across the beam as diffraction fringes. As the distance from the scatterer, R, increases the scattered part decreases (due to $\sim 1/\sqrt{r}$ dependence of the Hankel functions on r), and in the shadow behind the scatterer a bright small spot, discovered and called at the beginnings of the diffraction theory a Poisson spot, appears. Upon further increase in R the central Poisson spot is growing while the diffraction fringes seen across the incident beam are disappearing.

The dependence of the currents J_{I}, J_{S}, and J_{T} on ϕ is shown in Fig. 8, in log–log plot in Fig. 8a, while the relevant integrated scattered fluxes are shown in Fig. 8b. These plots are, in some sense, analogical to those presented in Figs. 3a, b. Due to the finite width of the incident beam the most of rapid oscillations of J_{T} at large scattering angles have been removed. Less rapid oscillations that are left represent specific properties of the scattering known as the forward diffraction peaks. These forward diffraction peaks are observed not only in the optical domains but also, for example, in high energy elastic collisions of elementary particles, see e.g. [10].

In this discussion the scattering was defined as a process in which the impinging particles are deflected and removed from the incident beam. To evaluate quantitatively those particles it is necessary to specify the incident beam in a more precise way. In particular, it is necessary to determine a transverse extension and cross-section of the incident beam. In this discussion it has been assumed that the transverse extension, y_{B}, of the incident beam, centered along the x axis, dependent on the position along the beam x, is determined by

$$|J_{\mathrm{I}}(x, y_{\mathrm{B}})| = |J_{\mathrm{I}}(x, 0)|/1000.$$

This definition of the beam extension is somehow arbitrary; but, as will be shown, small changes in the estimation of the beam extension do not cause any significant effects.

The extension of the beam, at the distance $R_0 = 3000$ from the scatterer, is shown in Figs. 8a and b by the dotted vertical lines placed at $\phi_{\mathrm{B}} = \arcsin y_B/R_0$. As it is seen, the scattered current represented by J_{S} is noticeable only inside the incident beam for $\phi < \phi_{\mathrm{B}}$, but there, according to the present discussion, J_{S} does not represent any particle current. Beyond this sector, for $\phi_{\mathrm{B}} < \phi < \pi - \phi_{\mathrm{B}}$ the

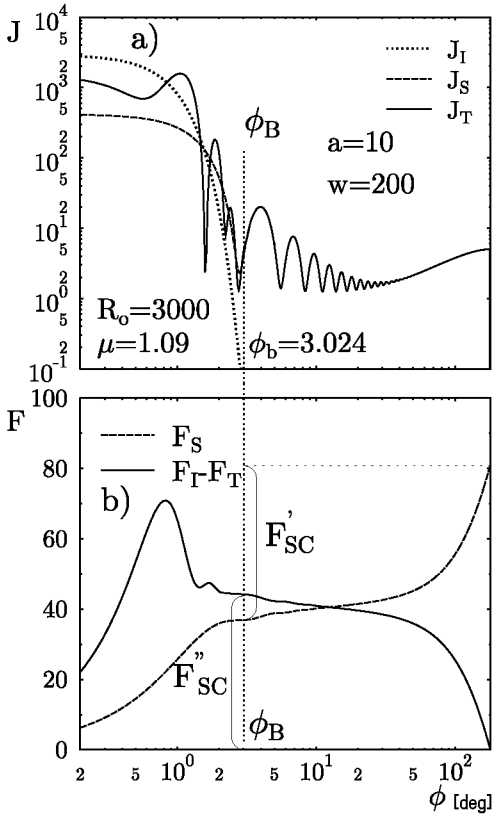

Fig. 8. (a) Incident, scattered and total radial currents for a beam wave scattering as functions of the scattering angle θ. (b) Scattered flux and the difference of incident and total fluxes as functions of θ. Measured scattered flux is defined either as $F'_{\rm SC} = F_{\rm S}(\pi) - F_{\rm S}(\phi_{\rm B})$ or $F''_{\rm SC} = F_{\rm I}(\phi_{\rm B}) - F_{\rm T}(\phi_{\rm B})$. F and J are in arbitrary units.

scattered current $J_{\rm S}(\phi)$ coincides with the true current $J_{\rm T}(\phi)$ determined by the total wave function.

To account the flux of particles removed from the incident beam one can either integrate the particle current outside that beam,

$$F'_{\rm SC}(R_0) = F_{\rm S}(R_0, \pi) - F_{\rm S}(R_0, \phi_{\rm B}),$$

or find the change of the particle flux inside the incident beam,

$$F''_{\rm SC}(R_0) = F_{\rm I}(R_0, \phi_{\rm B}) - F_{\rm T}(R_0, \phi_{\rm B}).$$

Figure 8b shows $F_{\rm S}(R_0, \phi)$ and $F_{\rm I}(R_0, \phi) - F_{\rm T}(R_0, \phi)$ in the entire range $0 \geq \phi \geq \pi$. As it appears from this picture, the two ways of calculation of the scattered fluxes give the same values, i.e., $F'_{\rm SC}(R_0) = F''_{\rm SC}(R_0)$.

The flux of particles scattered off the beam and detected as the scattered particles is equal to the reduction of flux of the incident beam measured across

its cross-section. This property can be identified with the optical theorem for the finite width beams. It does not depend on the precise definition and the value of the extension parameter for the incident beam. The curves showing $F_{\mathrm{S}}(R_0,\phi)$ and $F_{\mathrm{I}}(R_0,\phi) - F_{\mathrm{T}}(R_0,\phi)$ are mirror-like images in the horizontal line passing through their point of intersection, for ϕ greater than certain critical angle smaller than ϕ_{B}.

Using these definitions it is possible to determine how much the scattering flux determined according to the wave or the quantum theory differs from the corresponding classical scattering flux. A relevant parameter μ is

$$\mu = \frac{F^{\mathrm{Q}}_{\mathrm{SC}}(R_0)}{F^{\mathrm{C}}_{\mathrm{SC}}} = \frac{2F^{\mathrm{Q}}_{\mathrm{SC}}(R_0)}{F_{\mathrm{S}}(R_0,\pi)}. \tag{14}$$

The forward scattered beam at several distances R is shown in Fig. 9. It is characteristic how the initial rapid diffraction fringes, accompanying the shadow behind the scatterer, are vanishing, and the tiny Poisson spot that emerged in the shadow, grows and ends as the final beam. Its asymptotic shape resembles the attenuated incident Gaussian beam. The sixth graph of this figure is plotted at a distance at which a freely propagating Gaussian beam is naturally spread, due to diffraction, lowering its central intensity (notice the rescaled axes of this plot).

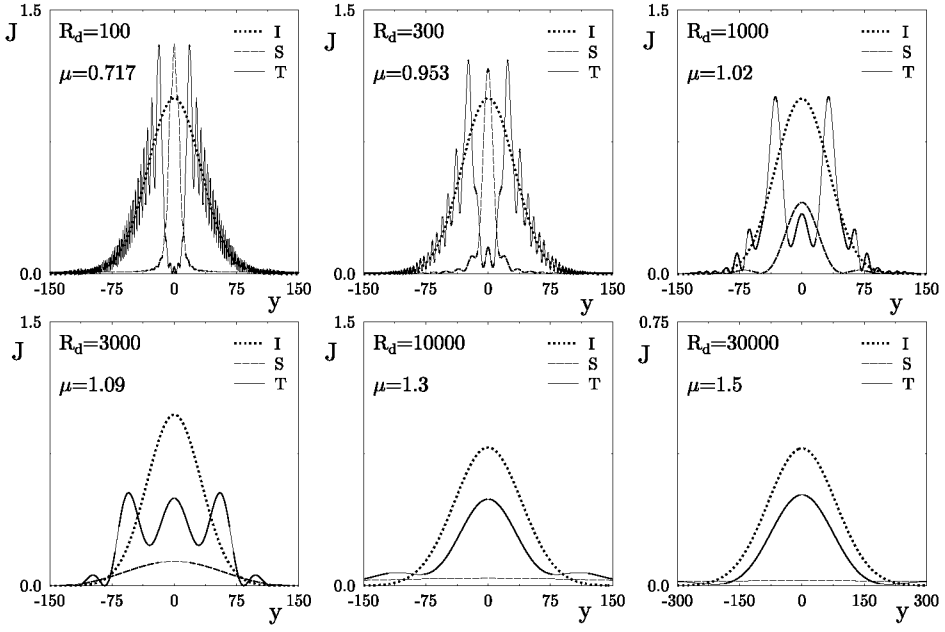

Fig. 9. Forward particle currents distributions at increasing distances from the scatterer. μ is the ratio of quantum and classical scattering fluxes ($a = 10,\ w = 200$). J and y are in arbitrary units.

The attenuated asymptotic beam experiences the same spreading. The remaining part of the beam can be recovered in the scattered particles outside the incident beam. It is worth pointing out that for increasing R the scattered flux and the associated parameter μ is also growing, reaching for the incident beam ($w = 200$) and scatterer radius $a = 10$ the final value $\mu = 1.5$. Further increase in R causes a proportional linear spreading of the incident and the scattered forward beam (notice the change of units in the last plot).

Similar effects are shown in Fig. 10, for a wider incident beam ($w = 1000$). In this case, the asymptotic distance above which the angular scattering pattern does not change is larger and the final value $\mu = 1.81$.

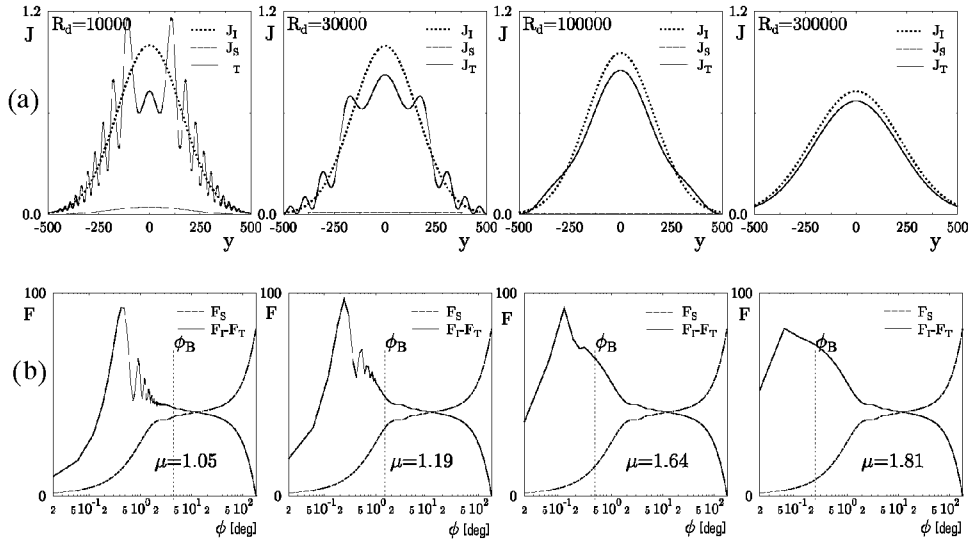

Fig. 10. (a) The same as in Fig. 9 for a wider beam, (b) scattered fluxes distributions and angular positions of the incident beam at various distances from the scatterer ($a = 10$, $w = 1000$). ϕ is in degrees, F in arbitrary units. F, J and y are in arbitrary units.

The bottom parts of these figures show how for increasing R the angular width of the beam boundary is decreasing and consequently shifting to the left. However, the angular width of the scattered beam is not vanishing. Otherwise our "optical theorem" would be violated. It remains finite, of the order of $\sim 1/w$, and within the range of the validity of the symmetry property for the functions $F_S(R_0, \phi)$ and $F_I(R_0, \phi) - F_T(R_0, \phi)$.

Considering the results presented in Figs. 9 and 10 it can be said that the classical scattered flux can be exceeded by the corresponding wave or the quantum flux when the width of the incident beam is greater than the diameter of the scatterer. In addition, the detection should be done sufficiently far away from the

scatterer, where the forward scattered beam shows no diffraction fringes and its shape resembles a distribution of the freely propagating incident beam at that place, reduced in its intensity due to scattering. For very wide beams, in the limit $w \to \infty$, the wave scattering factor $\mu \to 2$, and thus this scattering is very much different from the classical one. However, to observe these effects the measurement must be made sufficiently far away the scatterer, at distances $R > R_{\text{asy}}$. When $w \to \infty$ then $R_{\text{asy}} \to \infty$ shows that this limiting value $\mu = 2$ may only be detected asymptotically.

Another difficulty with the wide beam measurements in the forward direction is that the diminution of the incident beam due to scattering becomes negligible as compared with the total flux of the beam itself. Let us notice that even in the case shown in Fig. 10, the asymptotic shapes of the incident beam and the beam modified by scattering differ very little, and thus the observation of their difference would require measurements of very high accuracy.

Now, we can specify the classical limit in scattering supported by quantitatively verifiable arguments.

4. Classical limit in the scattering of waves

The classical dynamics as well as the classical scattering theory depend on the notion of particle trajectories or paths. However, it is difficult to introduce particle trajectories in the quantum mechanics when particles wave functions are given by plane waves or very wide beams. The particle trajectories can be associated with the wave functions corresponding to narrow Gaussian beams. These beams cannot be extremely narrow, because such beams are affected by a strong diffraction causing their rapid spreading. Only moderately narrow beams, of the width significantly larger than the de Broglie wavelength of the incident particles, stay narrow through the interaction region, and thus can be associated with the classical trajectories.

Accordingly, classical features of scattering can be expected for beams for which

$$1 \ll w \ll a. \tag{15}$$

When the above condition is fulfilled, one can introduce an impact parameter of scattered particles and connect the scattering angle (rather the mean scattering angle) with the impact parameter of the incident beam.

Three graphs in Fig. 11 illustrate the scattering of the incident beam of width $w = 10$ and displaced up to $y_0 = 30$ scattered by the cylinder of radius $a = 40$. It is obvious that in this case all the particles will be reflected (scattered) by this cylinder. These figures show shaded contour plots for modulus of the incident, scattered, and total currents, respectively. As it is shown in Fig. 11b the scattering current $\boldsymbol{J}_{\text{S}}$ consists of the two beams propagating outward the scatterer. One of

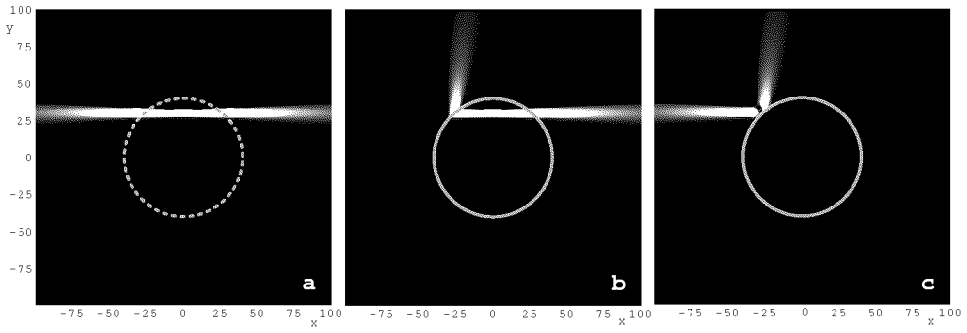

Fig. 11. Shaded contour plots of constant modulus of the currents: (a) incident ($|\boldsymbol{J}_{\mathrm{I}}|$), (b) scattered ($|\boldsymbol{J}_{\mathrm{S}}|$), (c) total ($|\boldsymbol{J}_{\mathrm{T}}|$) for the shifted narrow particle beam ($a = 40,\ w = 10$ and $y_0 = 30$).

them propagates from the scatterer along the incident beam, while the second one can be identified with a reflected beam. The integrated flux of each of these two beams are equal to the flux of the incident beam. Doubling the incident particle's flux by the above "scattered flux" shows, in the most convincing way, that, in situations when the scattered wave function Ψ_{S} overlaps with the incident wave function Ψ_{I}, $\boldsymbol{J}_{\mathrm{S}}$ cannot be interpreted as a particle current. A true particle current has to be computed using the total wave function Ψ_{T}. This particle current, $|\boldsymbol{J}_{\mathrm{T}}|$, presented in Fig. 11c, shows how in the specified conditions the entire particle beam is reflected from the scatterer.

For a such narrow beam scattering an impact parameter can be introduced and a relation between the mean scattering angle and the impact parameter can be established, similar to the corresponding relation in the classical theory. An additional reflected beam spreading is a very characteristic feature of the reflection of the beams by convex mirrors.

A similar classical feature of the wave and the quantum scattering of narrow beams can be illustrated by means of the particle flow lines determined by Eq. (9). These flow lines for a narrow beam scattered from a larger radius rigid cylinder are shown in Figs. 12a and b. While Fig. 12a gives a general view of the scattering flow, Fig. 12b shows its details in the region very close to the scatterer, where the beam reflection takes place. Although the general picture of the scattered flow resembles the corresponding classical trajectories, there is an important difference. The classical trajectories moving with smaller impact parameter are reflected stronger, and thus all scattered trajectories are intersecting. The quantum mechanical flow lines cannot intersect. Thus, in the classical and the quantum mechanics the relations between the incident and the outgoing parts of the flow lines are mutually inverted. However, an entire narrow beam behaves like a classical trajectory. Increasing the shift of the beam, i.e. increasing the impact parameter, the mean value of the scattering angle is decreasing.

Thus classical beams corresponding to an ensemble of randomly displaced

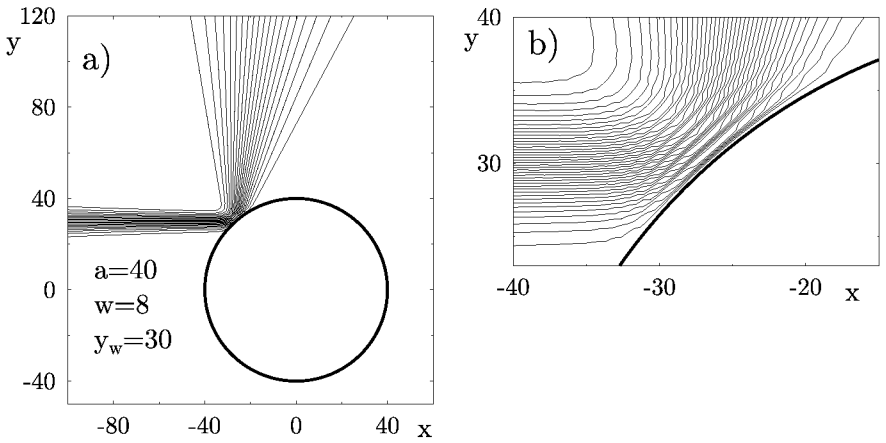

Fig. 12. (a) Energy flow lines for the same beam as presented in Fig. 11, (b) details of the same energy flow lines near the scatterer surface.

particles in the quantum mechanics can be represented by the analogical ensemble of randomly displaced narrow wave beams with the width w satisfying the condition $w \ll a$. Using such narrow wave beams as probe beams the classical procedure defining a scattering, differential cross-section and total cross-section could be adopted leading to the classical values for $\mathrm{d}\sigma^{\mathrm{C}}/\mathrm{d}\phi$ and σ_0^{C}.

5. Final remarks

The discussion of the "extinction paradox" has begun by a thorough analysis of the quantum theory of elastic scattering. Using the exact wave function for the two-dimensional scattering of a particle by a hard cylinder it was pointed out that an application of the standard quantum mechanical theories requires some caution in the description of the forward elastic scattering. These theories can be formulated in more consistent way if the plane waves, usually taken as incident wave functions, are replaced by the wave functions of finite width beams. Then, the scattering can be defined as a process of removing or scattering particles outside the beam caused by their interaction with the target particle introduced into the beam. This process is accompanied by adjusted modifications of the beam itself. The total flux of the scattered particles can be measured either by detectors placed outside the incident beam or by the change of the forward flux of the beam.

For a given size of the scatterer and width of the incident particle beam the angular patterns of the particle scattered outside the beam and the inside beam distribution stabilizes if the detectors are placed beyond certain characteristic distance R_{c} dependent on the beam width w and the scatterer size a. At these distances the shadow region seen just behind the scatterer is replaced by the attenuated, due to scattering, incident beam. When w grows the critical distance,

R_c increases and the attenuation of the forward radiation is decreasing, so its measurement, requiring higher accuracy detectors, becomes more difficult.

When $w \gg a \gg 1$ the flux of scattered particles can be twice larger than that one predicted by the classical theory.

The width parameter w should be connected with the transverse coherence length of the individual particles. Until now, in all macroscopic systems this transverse coherence length is always much smaller than a typical size of macroscopic scatterers (e.g. billiard balls). Therefore, these scatterings can be described classically.

This situation may change upon the construction of an atomic laser. Such atomic laser could provide atomic beams with w exceeding the size of scatterers for which the wave and the quantum scattering properties would become important. The above properties can be easily demonstrated with a laser pointer. While the reflection of these beams from any macroscopic mirror can be viewed classically in terms of geometrical optics, its scattering by a thin wire or needle requires the wave theory of scattering.

There is nothing paradoxical in an existence of the two extinctions — classical and quantum. Both extinctions refer to the two distinct preparations of the initial conditions and the final measurements, so one should not be surprised that the results are different. With a better understanding of the conditions for the quantum or the wave scattering it could be interesting to verify these results experimentally.

References

[1] A. Messiah, *Quantum Mechanics*, Interscience, New York 1961.

[2] L.I. Schiff, *Quantum Mechanics*, McGraw-Hill, New York 1968.

[3] I. Białynicki-Birula, M. Cieplak, J. Kamiński, *Theory of Quanta*, Oxford University Press, Oxford 1992.

[4] N.F. Mott, H.S.W. Massey, *The Theory of Atomic Collisions*, Clarendon Press, Oxford 1965.

[5] R.G. Newton, *Scattering Theory of Waves and Particles*, 2nd ed., Springer-Verlag, New York 1982.

[6] H.S.W. Massey, C.B.O. Mohr, *Proc. R. Soc. A* **141,** 434 (1933).

[7] J.D. Jackson, *Classical Electrodynamics*, Wiley, New York 1962.

[8] J.O. Hirschfelder, K.T. Tang, *J. Chem. Phys.* **65,** 470 (1976).

[9] W. Żakowicz, submitted to *Phys. Rev. E.*

[10] D.H. Perkins, *Introduction to High Energy Physics*, Polish Scientific Publishers PWN, Warsaw 1989 (in Polish).